Contents lists available at ScienceDirect

Agricultural and Forest Meteorology
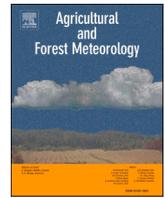
Spatio-temporal dynamics and controls of forest-floor evapotranspiration across a managed boreal forest landscape

Zifan Guo [a,b], Hengshuo Zhang [a,c,*], Eduardo Martínez-García [c,d], Xizhi Lv [a], Hjalmar Laudon [c], Mats B. Nilsson [c], Matthias Peichl [c]

[a] *Yellow River Institute of Hydraulic Research, Henan Key Laboratory of Yellow Basin, Ecological Protection and Restoration, Zhengzhou 450003, China*
[b] *School of Soil and Water Conservation, Beijing Forestry University, Beijing, 100083, China*
[c] *Department of Forest Ecology and Management, Swedish University of Agricultural Sciences, Skogsmarksgränd 17, 901 83, Umeå, Sweden*
[d] *Natural Resources Institute Finland (Luke), Latokartanonkaari 9, 00790, Helsinki, Finland*

ARTICLE INFO

ABSTRACT

Forest-floor evapotranspiration (ET_{ff}) is a major pathway for water loss in terrestrial ecosystems, often accounting for more than half of ecosystem evapotranspiration. However, our understanding of the environmental and stand structural controls on the spatio-temporal dynamics of ET_{ff} across the managed boreal forest landscape remains limited. In this study, we conducted chamber-based flux measurements of ET_{ff} and its components, i.e., soil evaporation (E_s) and forest-floor understory transpiration (T_u), on natural and vegetation removal plots across 50 diverse forest stands (ranging 5–211 years old) in Northern Sweden over two contrasting growing seasons. We found manifold variations in the growing season means of ET_{ff}, E_s, and T_u, ranging from 0.008 to 0.048 mm h^{-1}, 0.004 to 0.034 mm h^{-1}, and 0.002 to 0.030 mm h^{-1}, respectively, across the 50 forest stands. The contribution of E_s and T_u to ET_{ff} ranged from 19 to 83 % and 38 to 85 %, respectively, with the average E_s:T_u ratio shifting from 0.84 in 2017 to 0.63 during 2018, the latter experiencing an exceptional summer drought. Seasonal variations in ET_{ff} and its component fluxes were mainly controlled by below-canopy air temperature, while radiation was the main driver of their spatial variations across the forest stands. At the landscape-level, stand age was the dominant control of ET_{ff} by modifying overstory tree characteristics such as biomass and leaf area index. In contrast, neither tree species nor soil type had any effect on ET_{ff} or T_u. However, E_s was higher in sediment compared to till soils. Thus, our results suggest that environmental and stand structural factors jointly control the spatio-temporal dynamics of ET_{ff} across the managed boreal forest landscape. Our study furthermore highlights the need for an in-depth understanding of ET_{ff} and its components when assessing the water cycle feedbacks of the boreal forest to changes in forest management and climate.

1. Introduction

The boreal biome accounts for approximately 10–15 % of the global land area (Baldocchi and Vogel, 1996; Pan et al., 2011). The boreal forest is among the most vulnerable regions to climate change, with the potential for significant impacts on their water cycle (Liu et al., 2019; Helbig et al., 2020; Wang et al., 2021). Evapotranspiration (ET) is usually the main water loss in boreal forests, accounting for about 85 % of precipitation during the growing season (Kozii et al., 2020; Laudon et al., 2021). ET is composed of canopy interception, tree transpiration, and forest-floor evapotranspiration, but most studies in boreal forests only focus on exploring the dynamics and controls on tree transpiration (Barker et al., 2009; Chen et al., 2011; Gutierrez Lopez et al., 2021) and/or whole-ecosystem ET (McLaren et al., 2008; Kotani et al., 2014; Liu et al., 2020a; Jin et al., 2023; Hao et al., 2023). In comparison, there is limited information available on the role of forest-floor evapotranspiration (ET_{ff}) and its two main components, i.e., soil evaporation (E_s) and transpiration from the forest-floor understory vegetation (T_u). Hence, it is crucial to improve our understanding of the spatio-temporal dynamics of ET_{ff} and its environmental controls to better predict boreal forest water cycle-climate feedbacks.

In the boreal biome, forest canopies are relatively sparse, resulting in enhanced forest-floor understory development, which contributes significantly to the ecosystem water and carbon exchanges (Barker et al.,

2009; Kozii et al., 2020; Chi et al., 2021; Peichl et al., 2023a). Based on previous site-level studies, ET_{ff} in boreal forests may account for 8 % to 65 % of whole-ecosystem ET (Iida et al., 2009; Benyon and Doody, 2015). The spatio-temporal variability of ET_{ff} may be controlled by a range of below-canopy environmental factors, including solar radiation, air temperature, soil temperature, vapor pressure deficit, and soil water content. These factors interact with biological processes and properties inherent to vegetation, such as leaf area index and stomatal conductance (Kelliher et al., 1990; Zha et al., 2013; Numata et al., 2021). Furthermore, it is important to note that evaporation and transpiration are modulated by different sets of factors (Penman, 1963; Bosch et al., 2014; Zhang et al., 2017). Specifically, soil evaporation is a physical process primarily controlled by abiotic factors such as radiation energy, vapor pressure deficit, water availability in the topsoil, and the shading effects of the vegetation canopy (Penman and Keen, 1948; Magliano et al., 2017; Zhang et al., 2017). In contrast, plant transpiration operates within the soil-plant-atmosphere continuum and is regulated by both abiotic and biotic factors, including soil moisture accessible to plants in the root zone, vapor pressure deficit, leaf area index, and the physiological control of leaf stomata (Seemann et al., 1979; Shuttleworth, 1993; Iqbal et al., 2021; Chen et al., 2023a). Despite this well-established fundamental understanding, there is currently a lack of detailed knowledge on how the network of controlling factors is modulated across a heterogeneous boreal forest landscape.

Key forest stand attributes, including edaphic (i.e., soil type) and structural (i.e., tree species and stand age) properties, vary across the managed boreal forest landscape (Martínez-García et al., 2022; Peichl et al., 2023b), and thus have the potential to affect the spatial variability of ET_{ff}. For instance, ET_{ff} is commonly found to decrease with increasing tree canopy cover or leaf area index across different ecosystems or biomes (Iida et al., 2009). Canopy structural changes may also affect the microclimate at the forest-floor interface through canopy shading effects on soil moisture, temperature, and radiation levels (Monteith, 1990; Marques et al., 2020; Liu et al., 2022). Furthermore, different tree species have specific leaf area index and root water uptake characteristics, thereby altering ET_{ff} (Gao et al., 2022; Lyu et al., 2022; Chen et al., 2023b). Stand age may affect ET_{ff}, by influencing forest structure and microclimate conditions (Iida et al., 2009). Specifically, as forest stands age, increased canopy density and leaf area index result in reduced light penetration and below-canopy temperatures. Additionally, tree roots compete with forest-floor understory plants for soil water, which may affect both E_s and T_u.

Sediment and till soils exhibit distinct hydrologic properties that may affect ET_{ff} (Niu and Liu, 2022). Additionally, forest management activities (e.g., fertilization, thinning, drainage, and site preparation) affect species composition, canopy vertical structure, and soil properties, which may lead to increased spatial heterogeneity in ET_{ff} across the managed boreal forest landscape (Iida et al., 2009; Balandier et al., 2022; Kassuelke et al., 2022). The biophysical regulatory mechanisms, combined with the changing forest stand attributes throughout the heterogeneous landscape, result in remarkable temporal (at both seasonal and inter-annual scales) and spatial variations in ET_{ff} and its components (Kelliher et al., 1997; Baldocchi et al., 1997; Ohta et al., 2001; Hamada et al., 2004). Therefore, it is crucial to have a comprehensive understanding of the separate factors that control E_s and T_u, in order to reconcile how landscape properties, climate, and forest management in concert regulate ET_{ff} across the managed boreal forest landscape.

More frequent drought events are expected to be a significant global change factor that likely will modify ET_{ff} dynamics in the future (Constantin et al., 1999; Hamada et al., 2004; Yang et al., 2020). However, the consequences of drought have remained elusive due to its dual impact (Williams et al., 2013). Specifically, moderate increases in air temperature and vapor pressure deficit may lead to increased ET_{ff} (Iida et al., 2009). However, reduced soil water content and stomatal conductance beyond certain thresholds may eventually decrease both E_s

and T_u (Lafleur and Rouse, 1988; Liu et al., 2020b; Sabater et al., 2020). Furthermore, previous studies have reported that ET_{ff} may decrease during hydrological droughts (characterized by low soil water content), while it may increase during atmospheric droughts (marked by high vapor pressure deficit) (Iida et al., 2009). Therefore, improved knowledge is warranted to elucidate the impact of drought on boreal forest ET_{ff}.

In this study, chamber-based flux measurements were conducted to estimate ET_{ff}, E_s, and T_u in 50 forest stands across a managed boreal forest landscape located in northern Sweden over two growing seasons. These forest stands differed in soil type (sediment vs. till), dominant tree species (pine vs. spruce), and stand age (5–211 years). The objectives of this study were to: (1) investigate the magnitudes and variations of ET_{ff}, E_s, and T_u across a managed boreal forest landscape, (2) examine their sensitivity to forest stand attributes including edaphic (soil type) and structural (tree species and stand age) properties, and (3) determine the key biotic and abiotic factors regulating their spatio-temporal variability at the landscape-scale.

2. Materials and methods

2.1. Site description

The study was conducted within the Krycklan Catchment Study (KCS, Laudon et al., 2021), a long-term monitored catchment spanning 68 km^2 and located ca. 70 km northwest of Umeå (Sweden, 64°14′N, 19°46′E; Fig. 1). The climate is cold temperate humid with a 30-year (1991–2020) mean annual air temperature and total precipitation of 2.4 ± 0.3°C and 638 ± 40 mm, respectively. The terrain is gently undulating and spans elevations from 138 m a.s.l. at the catchment outlet in the southeastern part of the KCS to 339 m a.s.l. in the northwest. The forest stands include predominantly Scots pine (*Pinus sylvestris* L., 63 %) and Norway spruce (*Picea abies* (L.) H. Karst., 26 %) mixed with deciduous trees (mainly *Betula* spp., with minor contribution of *Alnus incana* (L.) Moench., and *Populus tremula* L., 11 %). The forest-floor understory layer consists mainly of ericaceous shrubs such as bilberry (*Vaccinium myrtillus* L.) and lingonberry (*Vaccinium vitis-idaea* L.) on moss mats of *Hylocomium splendens* (Hedw.) Br. Eur. and *Pleurozium schreberi* (Brid.) Mitt. Most of the forested area is managed by conventional clear-cut rotation forestry, i.e., with mainly even-aged stands which are mostly artificially regenerated and thinned.

We selected 50 forest stands spanning 5 to 211 years-old (average age of 73 ± 43 years) by stratification from a nominal regular grid (350 m × 350 m) of 556 permanent forest inventory plots located over the entire catchment (Fig. 1). Within each selected forest stand, the sample plot (10 m radius) belonging to the KCS plot-network was used for biometric- and chamber-based flux measurements. These forest stands were grouped into five age classes including initiation ($n = 8$), young ($n = 9$), middle-aged ($n = 13$), mature ($n = 14$), and old ($n = 6$), which ranged from 5 to 27, 31 to 58, 61 to 78, 80 to 105, and 131 to 211 years old, respectively. Additionally, each stand was classified according to soil type (sediment and till, $n = 15$ and 35, respectively) and dominant tree species (pine and spruce, $n = 28$ and 22, respectively). Key stand properties were determined for each forest stand based on biometric measurements, including tree aboveground biomass, understory aboveground biomass, understory belowground biomass, and leaf area index at peak growing season. See Table 1 for details on forest stands characteristics. The details on respective methods and data processing were previously described by Martínez-García et al. (2022).

2.2. Measurements of ET_{ff} and environmental variables

We established a split-plot design trenching experiment in late summer 2015 in each of the 50 forest stands, which was located 5 m outside from the boundary of the 10-m radius forest inventory plot to avoid disturbance from trampling and root trenching. This set up
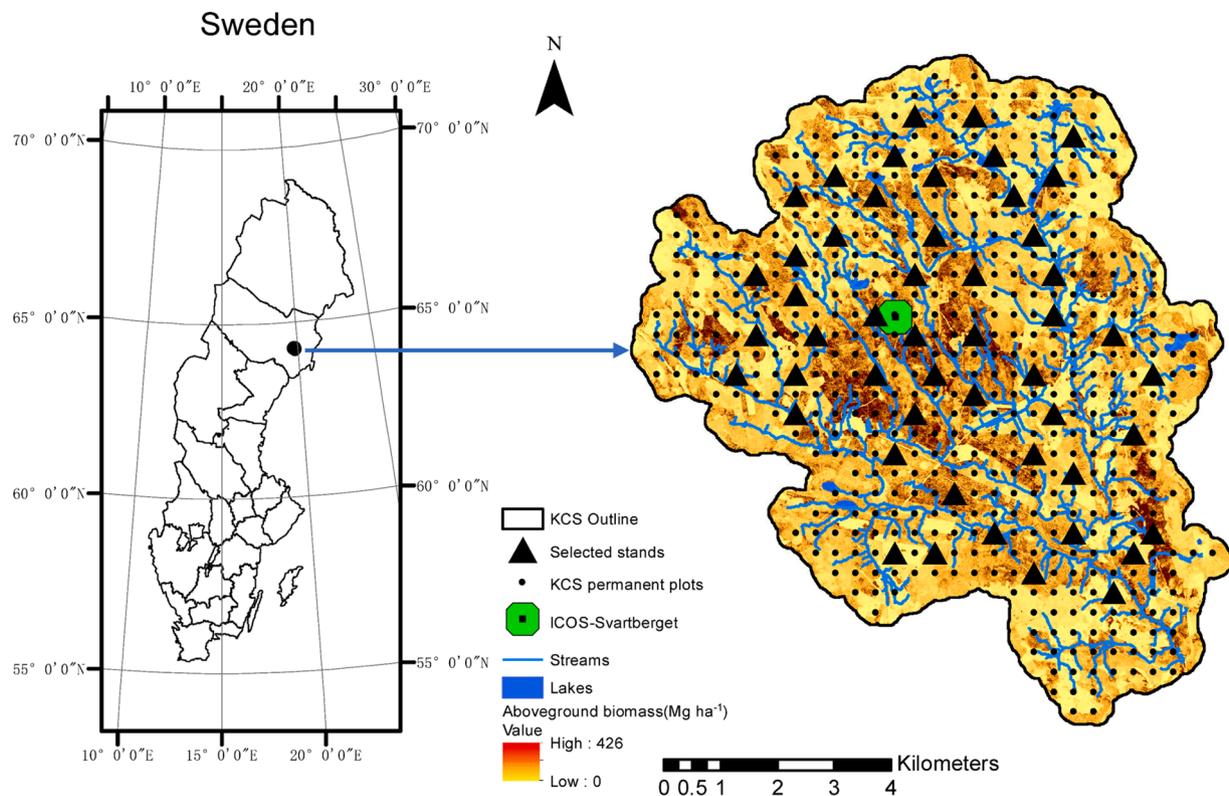
Fig. 1. Location map of the Krycklan Catchment Study (KCS) in northern Sweden. Detailed map displays the outline of the KCS, selected forest stands (triangles), KCS' network of permanent forest inventory plots (dots), ICOS-Svartberget (Integrated Carbon Observation System) Atmosphere-Ecosystem station (green dot) along with the light detection and ranging (LiDAR) derived estimates of aboveground biomass (data obtained from the Swedish University of Agricultural Sciences and Swedish Forest Agency). Lakes and streams within the KCS are also shown.

Table 1
Forest stand characteristics according to key forest stand attributes. Soil type: sediment (S) and Till (T), Tree species: Scots pine (SP) and Norway spruce (NS), Stand age: Initiation (I), Young (Y), Middle-aged (Ma), Mature (M), and Old (O). Td: tree density (trees ha^{-1}), BA: basal area (m^2 ha^{-1}), H$_t$: total tree height (m), B$_t$: total tree biomass (Mg ha^{-1}), B$_u$: total understory biomass (Mg ha^{-1}). Values represent the 2-year (2017−2018) mean with standard deviation in brackets.

Component	Soil type		Tree species		Stand age				
	S	T	SP	NS	I	Y	Ma	M	O
Td	928	1134	1080	1064	1045	1148	973	979	1423
	(292)	(627)	(576)	(537)	(378)	(505)	(544)	(427)	(891)
BA	17.4	22.3	19.6	22.5	3.7	17.6	20.5	26.8	35.5
	(11.4)	(10.7)	(11)	(11.2)	(3.2)	(6.7)	(5.9)	(7.6)	(6.2)
H$_t$	14.7	16.9	15.5	17.2	5.09	15.3	17.1	20.1	21.5
	(6.3)	(5.5)	(5.9)	(5.5)	(2.69)	(1.8)	(1.9)	(1.9)	(4.0)
B$_t$	102.7	140.0	111.6	150.8	12.3	93.8	123.3	174.4	242.4
	(82.0)	(81.0)	(91.5)	(19.5)	(9.5)	(42.2)	(36.5)	(56.8)	(78.3)
B$_u$	6.9	6.2	7.3	5.4	9.2	6.2	6.7	5.6	4.4
	(1.9)	(2.8)	(2.3)	(2.6)	(1.5)	(1.9)	(2.6)	(2.2)	(2.3)

included two adjacent plots (1 m^2), designated as natural (vegetated) and vegetation removal (non-vegetated) plots to quantify ET$_{ff}$ and E$_s$, respectively. The natural plot was selected to include a forest-floor understory vegetation cover and species composition representative of the 10-m radius forest inventory plot. It is important to note that the understory refers to the vegetation growing on the forest floor (i.e., lichens, herbs, mosses, and dwarf shrubs), but not understory trees. The vegetation removal plot was located within a few meters of the natural plot, and we further observed no significant effects of vegetation removal on soil volumetric water content at a 5 cm depth and soil temperature at a 10 cm depth, e.g., through reduced root water uptake, shading, and interception (Fig. S1).

Subsequently, T$_u$ was estimated as the difference between ET$_{ff}$ and E$_s$. It should be noted that the difference between ET$_{ff}$ and E$_s$ also includes the evaporation of intercepted precipitation from the forest-floor

understory (E$_u$). However, since H$_2$O flux measurements were carried out during generally drier midday hours and not during rainy days, the contribution of E$_u$ was likely minor and the difference between ET$_{ff}$ and E$_s$ was therefore considered to represent T$_u$ in our study.

In the center of each natural and vegetation removal plots, one square chamber base frame (aluminium, 0.2025 m^2 area, 0.05 m height) was embedded 1–2 cm into the soil surface to facilitate H$_2$O flux measurements. H$_2$O fluxes were determined using a custom-made closed steady-state chamber (45 × 45 cm width, 20 cm height, 5 mm thick transparent acrylic Plexiglas® with 8 % light attenuation). The chamber dimensions were sufficient to contain the forest-floor understory vegetation typically found in the study plots. The chamber was connected to a portable infrared gas analyser (LGR-GGA-24EP, Los Gatos Research Inc., San Jose, CA, USA; GasScouterTM G4301, Picarro, Santa Clara, CA, USA) in a closed sampling loop to determine changes in the H$_2$O

concentration within the chamber headspace during chamber placement. Between measurements, the sample tubing was dried by flushing with ambient air until the H_2O concentration returned to its original ambient baseline values. ET_{ff} was measured with a transparent chamber under ambient daylight conditions, whereas the chamber was covered with an opaque tarp during the measurement of E_s. The latter was done since soil carbon dioxide fluxes were measured simultaneously for another study (Martínez-García et al., 2022), with the assumption that the absence of light does not affect E_s.

H_2O fluxes were measured monthly at each forest stand from May to October during 2017−2018. Within each monthly sampling, 5–7 forest stands were measured per day between 8:00−16:00h over the course of 7–9 days. A random order among the 50 forest stands was applied in each H_2O sampling to prevent diurnal effects. The measurement was conducted over a short period of 90–120 s on each frame to limit fluctuations in air pressure and temperature changes within the chamber. A period of at least two minutes was allocated for venting between measurements to allowed for the equalization of the H_2O concentration and air pressure inside with that outside the chamber.

During each H_2O flux measurement, below-canopy air temperature was determined using a handheld digital thermometer (M514B, Sunartis, Mingle Instruments GmbH Europe, North Rhine-Westphalia, Germany), while below-canopy photosynthetic photon flux density was manually measured at each forest stand with a quantum sensor (QSO-S, Apogee Instruments Inc., Logan, UT, USA). It should be noted that net radiation is commonly considered as the key control of ET, as evidenced by its inclusion in the Penman-Monteith model (Penman and Keen, 1948). However, due to the lack of below-canopy net radiation data, this study employed photosynthetic photon flux density as a proxy. This was corroborated by the strong correlation ($R^2 = 0.97$, $P < 0.001$) observed between both variables (Fig. S2). Additionally, soil temperature at 10cm depth (soil temperature) was recorded using the handheld digital thermometer described above, and soil volumetric water content at a 5 cm depth (soil volumetric water content) was recorded using a moisture sensor (GS3, METER Group Inc., Pullman, WA, USA) at each forest stand.

Below-canopy vapour pressure deficit during each H_2O flux measurement was derived from measurements of below-canopy air temperature (Ta_{bc}) and initial H_2O concentration ($H2O_{conc}$, mmol mol^{-1} or ppm for Picarro and LGR analyzers, respectively) inside the chamber. First, the saturation vapour pressure (P_{ws}, kPa) was estimated from Ta_{bc} using Eq. (1).

$$P_{ws} = \left(6.1164 \times 10^{(7.5914 \times Ta_{bc}/240.7263+Ta_{bc})}\right)/10 \qquad (1)$$

Subsequently, atmospheric pressure (P, kPa) data from the ICOS-Svartberget (Integrated Carbon Observation System) Atmosphere-Ecosystem station (64°15′N, 19°46′E, 257 m a.s.l.) was used to calculate the water vapour pressure (P_w, kPa) from $H2O_{conc}$ and P using Eq. (2).

$$P_w = \left((H2O_{conc} \times P)/(H2O_{conc} + 10^6)\right)/10 \qquad (2)$$

Finally, the below-canopy vapour pressure deficit was estimated by subtracting P_w from P_{ws}.

2.3. Flux calculations and quality control

Forest-floor H_2O fluxes were calculated from the linear change in the headspace gas concentration over time corrected for air density using the ideal gas law (Livingston and Hutchinson, 1995) (Eq. (3)):

$$F_{H2O} = \left(\frac{d[H_2O]}{dt}\right) \times \left(\frac{P \times V}{R \times T \times A}\right) \qquad (3)$$

where F_{H2O} is the instantaneous H_2O flux (mmol H_2O m^{-2} s^{-1}), d[H_2O]/dt is the rate of change in water vapor-corrected H_2O concentration in the chamber headspace (i.e., slope; mmol mol^{-1} s^{-1}) derived from a linear fit, P is the air pressure inside the chamber (Pa, set to a constant value of 101325 Pa), V is the chamber volume (m^3), R is the universal gas constant (8.3143 J mol^{-1} K^{-1}), T is the air temperature at chamber closure (K), and A is the area inside the chamber base frame (m^2). After applying a 20 seconds 'dead band' to discard the initial records that were possibly prone to disturbance following chamber placement, the slope of the linear fit was computed from the following 30 seconds of concentration records (at 1 Hz sampling), following previous studies highlighting the need for short sampling periods to avoid bias due to water vapor adhesion to the sampling tubing (McLeod et al., 2004; Hamel et al., 2015).

The quality control procedure entailed a composite assessment based on both the root mean square error (RMSE) and R^2 as indicators of goodness of fit. Specifically, measurements with an $R^2 < 0.90$ and RMSE > 75 (LGR) or > 500 (Picarro) ppm H_2O were discarded. Additionally, negative measurements, which indicate implausible H_2O uptake, and notable outliers observed concurrently in both exponential regressions of H_2O vs below-canopy air temperature and soil volumetric water content, were also discarded. In total, 15 % of the H_2O flux data were removed due to the quality filtering processes. To reduce bias resulting from data gaps, a gap-filling procedure following Martínez-García et al. (2022) was executed to substitute ET_{ff} and E_s missing data at each forest stand. The procedure was based on the extrapolation of linear regressions between the measured ET_{ff} and E_s fluxes. For this purpose, the time series of each H_2O flux was compared with the time series of the other flux component at a given stand and the best linear equation (with the highest R^2) was selected for gap filling. When both H_2O fluxes were absent on a given sampling day, exponential regressions were employed for each H_2O flux in relation to below-canopy air temperature and/or soil volumetric water content, which were separately defined at for each forest stand.

2.4. Statistical analysis

All statistical analyses were performed using R (version 4.2.0; (R Core Team)) and R Studio (version 4.2.0) software. Data sets of two-year (2017–2018) mean annual values were tested prior to analysis for normality (Kolmogorov–Smirnov test) and homogeneity of variance (Levene's test) and log-transformed when necessary. One-way analysis of variance (ANOVA) was used to explore the effects of soil type, tree species, and stand age on ET_{ff}, E_s, and T_u fluxes. Tukey's Honestly Significant Difference (HSD) was used for pairwise comparisons. Linear, exponential, polynomial, and logarithmic regressions were defined to detect controls for the temporal dynamics of ET_{ff}, E_s, and T_u, where the determination coefficient (R^2) and root mean square error (RMSE) were used to determine the model with the best goodness of fit. Linear regression analysis using the *stats* package in R was employed to analyze the effects of forest stand attributes and to determine the effects of biotic and abiotic factors on the spatial dynamics of ET_{ff}, E_s, and T_u. The relative importance of abiotic controls in regulating ET_{ff} its components was examined using a stepwise generalised linear model (GLM) with log-link and gamma distribution. To identify the direct and indirect effects of biotic and abiotic factors on the spatial variations of ET_{ff}, E_s, and T_u, a structural equation model (SEM) was adopted to understand the relationships among tree aboveground biomass, understory aboveground biomass, understory belowground biomass, leaf area index at peak growing season, below-canopy photosynthetic photon flux density, air temperature and soil temperature based on 2-year (2017−2018) mean annual and growing season values across the 50 forest stands. Due to the high degree of covariance between below-canopy vapour pressure deficit and air temperature (Fig. S3), and the greater control of air temperature over vapour pressure deficit on ET_{ff}, we finally did not include vapour pressure deficit in our SEM model. The overall goodness of fit of our model is characterised by a non-significant chi-square test ($p > 0.05$), low root mean square error of approximation (RMSEA < 0.05), high Tucker–Lewis index (TLI > 0.90) and high comparative fit index

(CFI > 0.95). We also tested the effect of previous environmental and stand structural variables on the spatial variation in ET_{ff}, E_s, and T_u in a model of mixed-effects meta-regression using the *glmulti* package in R. The importance of each variable was determined as the sum of Akaike weights for models that included this variable, which can be considered as the overall support for each variable across all models. Statistical significance was set at $p \leq 0.05$.

3. Results

3.1. Temporal variations in environmental conditions

Averaged across all stands, below-canopy photosynthetic photon flux density, vapour pressure deficit, air temperature, soil temperature and soil volumetric water content showed different between-year variations (Fig. 2a–e), with seasonal mean air temperature being significantly higher in the drought year 2018 than in 2017, while seasonal mean soil volumetric water content showed the opposite pattern ($P < 0.05$). Seasonal means of below-canopy photosynthetic photon flux density, vapour pressure deficit, air temperature, soil temperature, and soil volumetric water content were 245 μmol photons m^{-2} s^{-1}, 0.34 kPa, 13.5 °C, 8.3 °C, and 0.32 m^3 m^{-3}, respectively, in 2017. In contrast, these values were 267 μmol photons m^{-2} s^{-1}, 0.75 kPa, 17.7 °C, 10.1 °C, and 0.23 m^3 m^{-3}, respectively, in 2018. Mean below-canopy photosynthetic photon flux density ranged from 82 to 393 μmol photons m^{-2} s^{-1} in 2017 and from 92 to 415 μmol photons m^{-2} s^{-1} in 2018 (Fig. 2a). Mean below-canopy vapour pressure deficit varied from 0.08 to 0.74 kPa in 2017 and from 0.08 to 0.77 kPa in 2018 (Fig. 2b). Mean below-canopy air temperature and soil temperature increased in all years from early in

the growing season, reached their respective maxima at mid-growth, and declined thereafter (Fig. 2c and d). Mean soil volumetric water content was higher at the beginning and at the end of the growing season with a temporary decrease during the peak summer. Mean soil volumetric water content varied from 0.28 to 0.37 m^3 m^{-3} in 2017 and varied from 0.16 to 0.29 m^3 m^{-3} in 2018 (Fig. 2e).

3.2. Temporal variations in forest-floor H_2O fluxes

ET_{ff}, E_s, T_u and the T_u/ET_{ff} ratio averaged across the 50 forest stands showed clear seasonal cycles and large between-year variations (Fig. 3a and b). Specifically, seasonal mean ET_{ff}, E_s, T_u and T_u/ET_{ff} ratio were significantly higher in the drought year 2018 than in 2017 ($P < 0.05$). ET_{ff} averaged across the 50 forest stands ranged from 0.006 to 0.048 mm h^{-1}, with a seasonal means of 0.014 ± 0.009 mm h^{-1} and 0.034 ± 0.02 mm h^{-1} in 2017 and 2018, respectively. Additionally, E_s averaged across the 50 forest stands ranged from 0.004 to 0.02 mm h^{-1}, with a seasonal means of 0.007 ± 0.004 mm h^{-1} and 0.014 ± 0.008 mm h^{-1} in 2017 and 2018, respectively. Meanwhile, T_u averaged across the 50 forest stands ranged from 0.007 to 0.032 mm h^{-1}, with a seasonal means of 0.008 ± 0.007 mm h^{-1} and 0.023 ± 0.018 mm h^{-1} in 2017 and 2018, respectively. At seasonal scale, the T_u/ET_{ff} ratio ranged between 0.40 and 0.61, with a lower seasonal mean of 0.49 in 2017 compared to 0.57 in 2018. In comparison, the E_s/ET_{ff} ratio ranged between 0.39 and 0.61, with a higher seasonal mean of 0.53 in 2017 compared to 0.44 in 2018 (Fig. 3b). Thus, the drought conditions shifted the partitioning of ET_{ff} towards higher T_u relative to E_s.
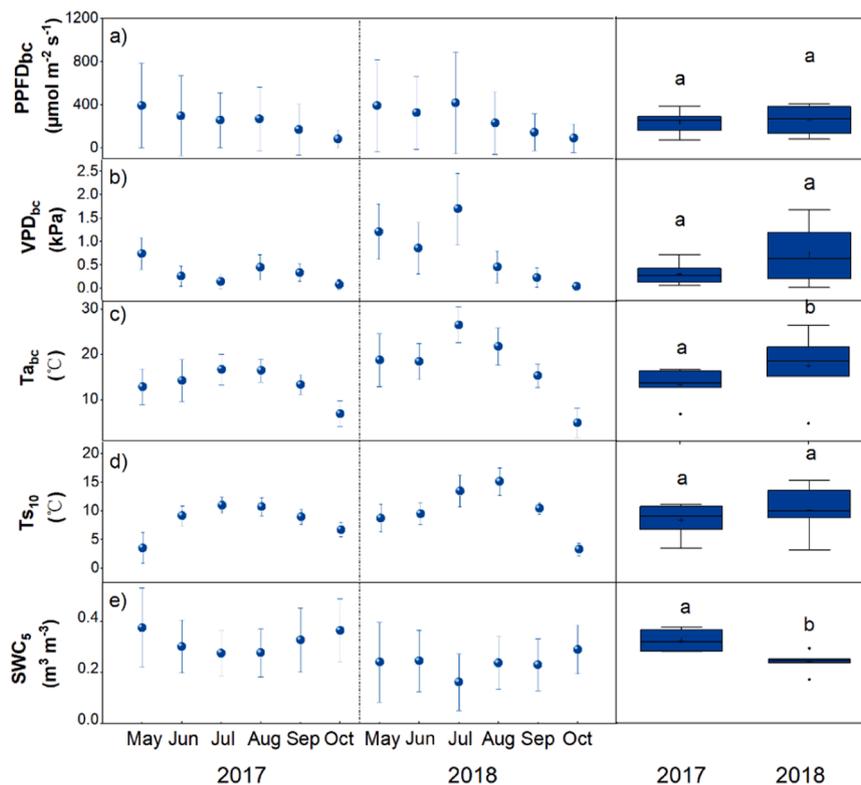
Fig. 2. Temporal variations in below-canopy environmental conditions including a) photosynthetic photon flux density ($PPFD_{bc}$), b) vapor pressure deficit (VPD_{bc}), c) mean air temperature (Ta_{bc}), d) soil temperature at 10 cm depth (Ts_{10}), and e) soil volumetric water content at 5 cm depth (SWC_5) averaged over the 50 forest stands for each measurement campaign from May to October during 2017–2018. Left-hand panels show mean values (standard deviation in error bars) of each variable 8. Right-hand panels show box plots with the mean annual values of each variable for each study year. Box plots represent the 25th (bottom) and 75th (top) percentiles, the central line represent the median, and the cross represent the mean. Whiskers above and below and the boxes represent data within 1.5 times the interquartile range, and outliers are given as individual points. The different letters above box plots within each variable indicate significant differences between years 2017 and 2018 (HSD test, $P < 0.05$). $n = 50$ forest stands.

Fig. 3. Temporal variations in a) forest-floor evapotranspiration (ET_{ff}, mm h^{-1}), soil evaporation (E_s), and forest-floor understory transpiration (T_u, mm h^{-1}), and b) the ratios of T_u to ET_{ff} and E_s to ET_{ff} averaged over the 50 forest stands for each measurement campaign from May to October during 2017–2018. Left-hand panels show mean values (standard deviation in error bars) of each variable. Right-hand panels show box plots with the mean annual values of each variable for each study year. Box plots represent the 25th (bottom) and 75th (top) percentiles, the central line represent the median, and the cross represent the mean. Whiskers above and below and the boxes represent data within 1.5 times the interquartile range, and outliers are given as individual points. The different letters above box plots within each variable indicate significant differences between years 2017 and 2018 (HSD test, $P < 0.05$). $n = 50$ forest stands.

3.3. Environmental controls on seasonal variations in ET_{ff}, E_s, and T_u

ET_{ff}, E_s, and T_u showed positive exponential relationships with below-canopy air temperature (Fig. 4c, h and m) and soil temperature (Fig. 4d, i and n), while photosynthetic photon flux density and vapor pressure deficit exerted an asymptotical control on ET_{ff}, E_s, and T_u (Fig. 4a, b, f, g, k and l). In contrast, soil volumetric water content explained the variations in ET_{ff}, E_s, and T_u through a negative asymptotical relationship (Fig. 4e, j and o). See Table S1 for further details on the coefficients of the equations. It should be noted that below-canopy photosynthetic photon flux density, vapor pressure deficit, air temperature and soil temperature were negatively correlated with soil volumetric water content (Fig. S4), whereas air temperature was positively correlated with vapor pressure deficit (Fig. S3).

The results of the stepwise GLM analysis further revealed that below-canopy photosynthetic photon flux density, vapor pressure deficit, air temperature, soil temperature and volumetric water content were the main temporal controls of ET_{ff} (Table 2). Additionally, the results indicated that air temperature and photosynthetic photon flux density were the primary controlling factors of T_u and E_s, with soil volumetric water content also exerting an influence on the latter (Table 2). Furthermore, this analysis corroborated the positive and/or negative correlations between H$_2$O fluxes and environmental variables presented in Fig. 4.

3.4. Effect of key forest stand attributes on spatial variations in ET_{ff}, E_s, and T_u

No effect of soil type and tree species was apparent on ET_{ff} and T_u (Fig. 5a, b, g and h). In contrast, E_s was significantly higher in sediment compared to till soils, but it did not differ among tree species (Fig. 5d and e). In addition, ET_{ff}, E_s, and T_u decreased significantly with stand age ($P < 0.05$) by about 50 % from 0.033 to 0.017 mm h^{-1}, 0.015 to 0.008 mm h^{-1}, and 0.022 to 0.01 mm h^{-1} from initiation to old stand age classes, respectively (Fig. 5c, f and i). Our results further show that the E_s/ET_{ff} and T_u/ET_{ff} ratios were not significantly affected by soil type,

tree species, and stand age ($p > 0.05$) (Fig. 5i–o).

3.5. Stand structural and environmental controls of ET_{ff}, E_s, and T_u at the landscape-scale

Our analysis revealed that at the landscape-scale, the seasonal mean ET_{ff} and its component fluxes E_s and T_u significantly decreased with increasing stand age, leaf area index at peak growing season, and tree aboveground biomass, but increased with increasing understory above- and belowground biomasses, below-canopy photosynthetic photon flux density, vapor pressure deficit, air temperature, and soil temperature ($P < 0.05$, Fig. 6). Among these various factors, photosynthetic photon flux density explained most of the spatial variations for each ET_{ff}, E_s, and T_u. It should also be noted that the explanatory power of each of the included factors was higher for E_s than for T_u. Besides, we found that below-canopy photosynthetic photon flux density, vapor pressure deficit, air temperature, soil temperature, leaf area index and tree aboveground biomass were negatively correlated with soil water content across 50 forest stands (Fig. S5). We further noted a significant decline in ET_{ff} and E_s with increasing thickness of the topsoil organic layer (Fig. S6).

The results of the SEM model further suggested that below-canopy photosynthetic photon flux density was the main control for the spatial variations in ET_{ff} and T_u across the managed boreal forest landscape. In addition, understory above- and belowground biomasses were additional important factors controlling ET_{ff} and T_u (Fig. 7a, b, e and f). Specifically, our SEM revealed a direct relationship ($P < 0.05$) among ET_{ff} and photosynthetic photon flux density and understory above- and belowground biomasses with the standardized coefficients being 0.61, 0.29 and 0.37 respectively. However, tree aboveground biomass suppressed ET_{ff} and T_u by increasing leaf area index (normalized coefficient = 0.87, $P < 0.05$). The SEM also showed that in addition to the dominant effect of below-canopy photosynthetic photon flux density, air temperature (0.24) plays an equally significant role in controlling E_s (Fig. 7c and d), whereas understory aboveground biomass (0.44) was the second
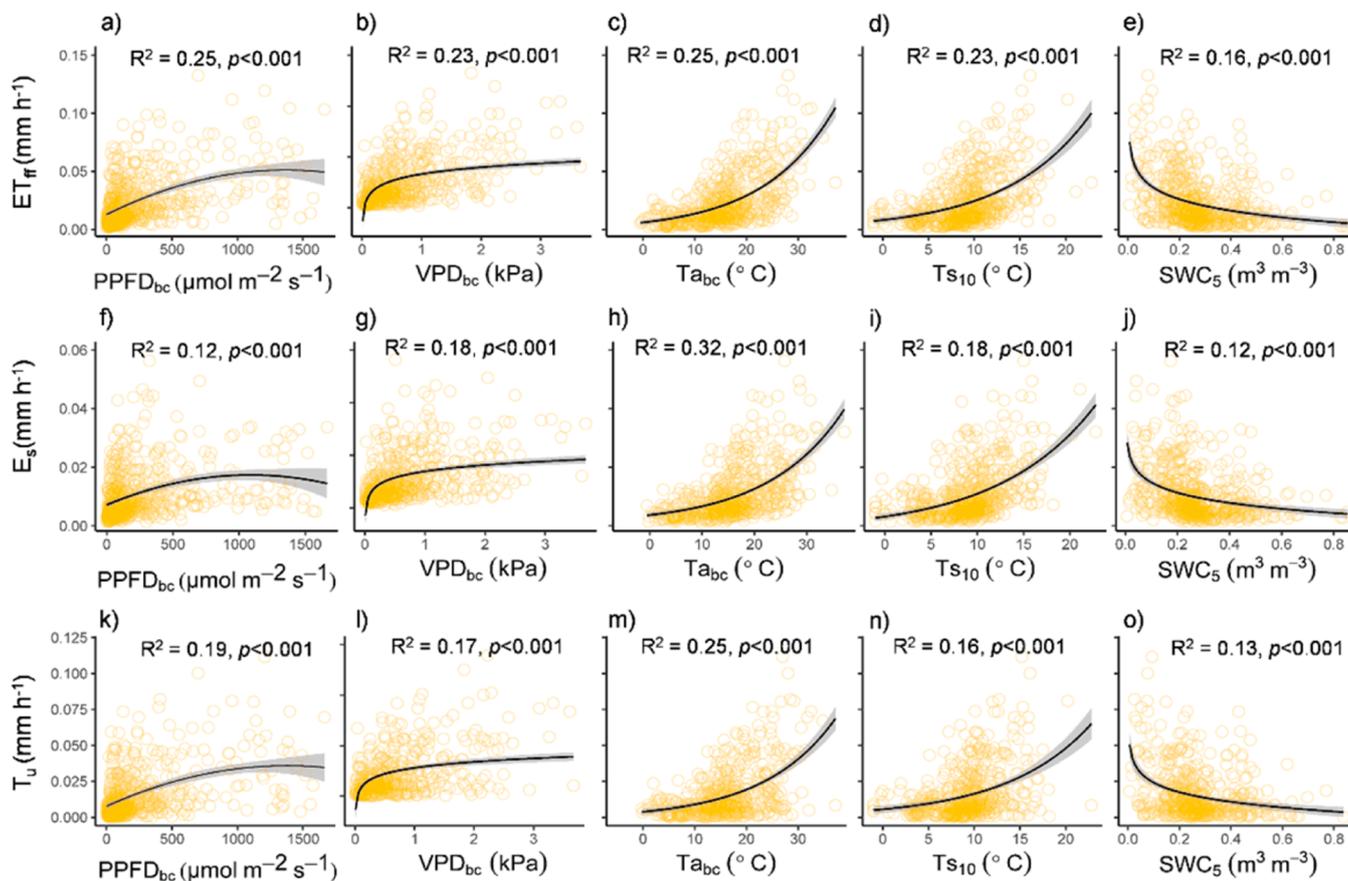
Fig. 4. Relationships of instantaneous forest-floor evapotranspiration (ET_{ff}, mm h^{-1}), soil evaporation (E_s, mm h^{-1}), and forest-floor understory transpiration (T_u, mm h^{-1}) with (a, f, and k) below-canopy photosynthetic photon flux density ($PPFD_{bc}$), (b, g, and i) below-canopy vapor pressure deficit (VPD_{bc}), (c, h, and m) below-canopy air temperature (Ta_{bc}), (d, i, and n) soil temperature at 10 cm depth (Ts_{10}) and (e, j, and o) soil volumetric water content at 5 cm depth (SWC_5) across the 50 forest stands. Dots and lines represent individual growing season values and non-linear regression fit lines, respectively. The gray area refers to the 95 % confidence interval for the regression line. Coefficient of determination (R^2) and p-value are shown. $n = 600$ (50 forest stands x 2 years [2017 and 2018] x 6 measurement campaigns per year).

Table 2

Generalized linear regression model results for environmental factors explaining seasonal variations of ET_{ff}, E_s, and T_u. Abbreviations: ET_{ff}, forest-floor evapotranspiration; E_s, soil evaporation; T_u, forest-floor understory transpiration; $PPFD_{bc}$, below-canopy photosynthetic photon flux density; VPD_{bc}, below-canopy vapor pressure deficit; Ta_{bc}, below-canopy air temperature; Ts_{10}, soil temperature at 10 cm depth; SWC_5, soil volumetric water content at 5 cm depth; Coeff., coefficient; and SE, standard error. Coefficient values are proportional to their effect size. Non-significant variables are indicated as n.s. Coefficient of determination (R^2) is also shown. $n = 600$ (50 forest stands x 2 years [2017 and 2018] x 6 measurement campaigns per year).

Variables	ET_{ff} $R^2 =$ 0.47 $n = 600$ Coeff.	SE	E_s $R^2 =$ 0.37 $n = 600$ Coeff.	SE	T_u $R^2 =$ 0.27 $n = 600$ Coeff.	SE
$PPFD_{bc}$	1.69e-05	2.16e-06	2.77e-06	9.52e-07	1.59e-05	2.08e-06
VPD_{bc}	4.85e-03	1.95e-03	n.s.	n.s.	n.s.	n.s.
Ta_{bc}	9.32e-04	2.24e-04	6.66e-04	1.00e-04	6.85e-04	2.19e-04
Ts_{10}	8.79e-04	2.69e-04	n.s.	n.s.	n.s.	n.s.
SWC_5	-1.22e-02	5.37e-03	-7.68e-03	2.45e-03	n.s.	n.s.

most important control on T_u (Fig. 7e and f). The driving factors in combination explained 60 %, 44 % and 51 % of the variations in ET_{ff}, E_s, and T_u, respectively.

4. Discussion

Our results reveal significant spatial and temporal variability in ET_{ff} in response to a combination of environmental and stand structural gradients across the studied managed boreal forest landscape. This highlights the need for a detailed understanding of the spatial and temporal mechanisms that control ET_{ff} to improve process-based models for better prediction of the interactions among the boreal forest water cycle, forest management, and climate change.

4.1. Dynamics of forest-floor H$_2$O fluxes across a managed boreal forest landscape

Compared to previous studies carried out in boreal ecosystems, our estimate of the mean growing season ET_{ff} (0.024±0.009 mm h^{-1}) obtained across 50 boreal forest stands was higher (0.013, Baldocchi et al., 1997; 0.013, Constantin et al., 1999), similar (0.021, Ohta et al., 2001), and/or lower (0.033, Kelliher et al., 1998; 0.033, Hamada et al., 2004). However, the wide range of ET_{ff} observed across our managed forest landscape (0.008 to 0.048 mm h^{-1}) encompasses the rates from these previous studies. It further indicates that the nearly 3-fold difference between the lowest and highest ET_{ff} rates reported across boreal forest stands is likely attributable to variations in site conditions (e.g., local
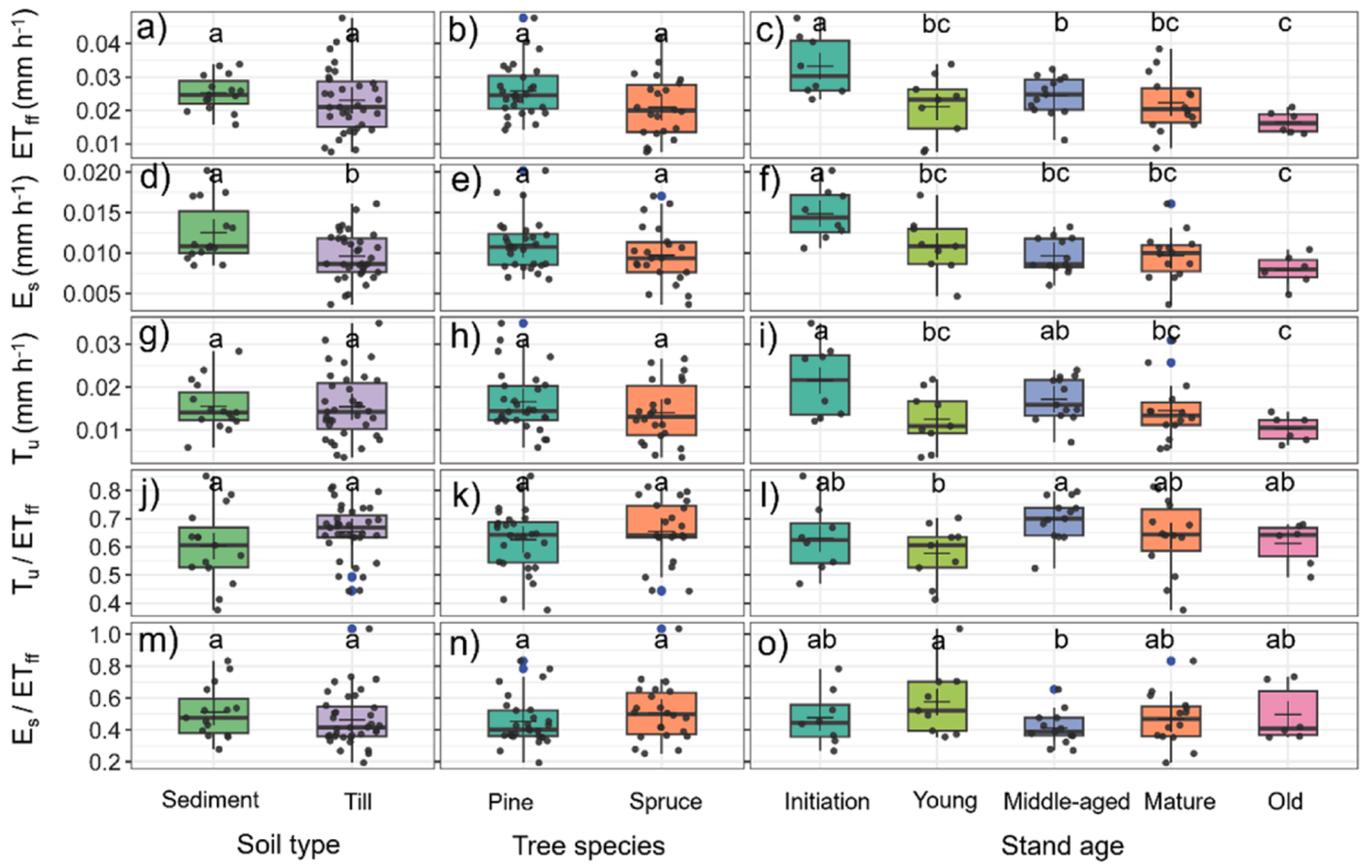
Fig. 5. Effect of soil type, tree species, and stand age on a)-c) forest-floor evapotranspiration (ET_{ff}, mm h^{-1}), d)-f) soil evaporation (E_s, mm h^{-1}), g)-i) and forest-floor understory transpiration (T_u, mm h^{-1}), j)-l) ratio T_u to ET_{ff}, and m)-o) ratio E_s to ET_{ff}. The different letters above box plots within each variable indicate significant differences between each forest stand attribute (HSD test, $P < 0.05$). Data based on 2-year (2017−2018) mean growing season values. The boxes represent the 25th (bottom) and 75th (top) percentiles, the central line the median, and the cross the mean. Whiskers above and below the boxes represent data within 1.5 times of the interquartile range and outliers are given as individual blue points.
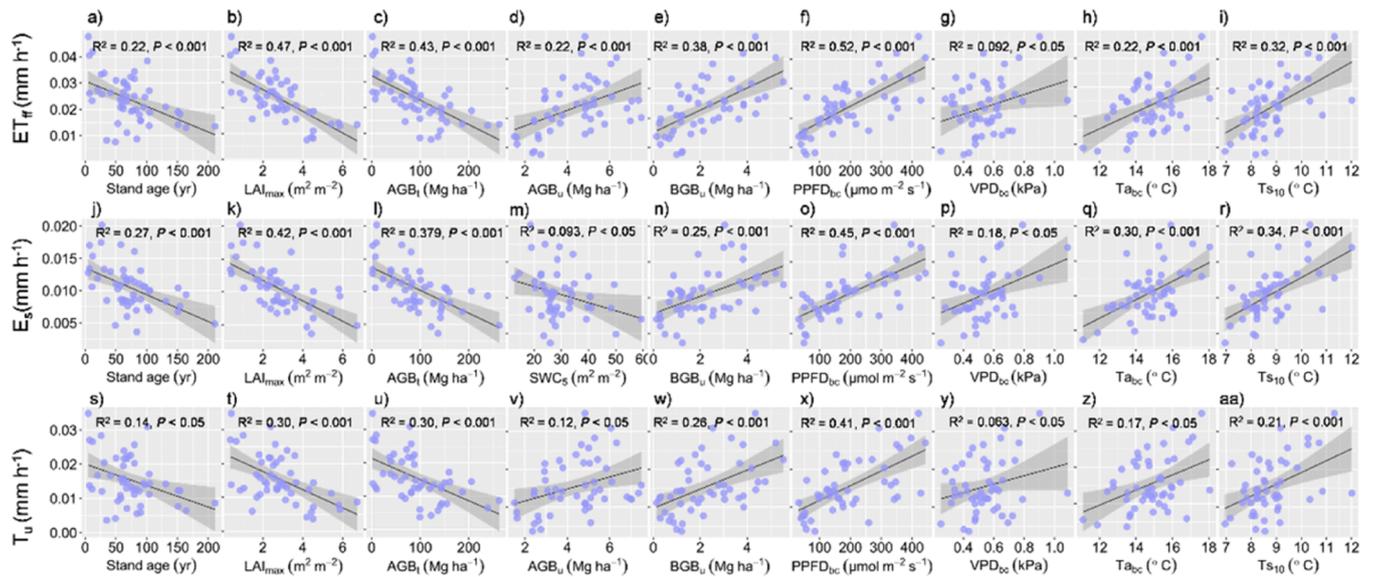
Fig. 6. Relationship of mean seasonal forest-floor evapotranspiration (ET_{ff}, mm h^{-1}), soil evaporation (E_s, mm h^{-1}), and forest-floor understory transpiration (T_u, mm h^{-1}) with stand structural and environmental controlling factors. Stand age (years), LAI_{max}: leaf area index at peak growing season, AGB_t: tree aboveground biomass; AGB_u: understory aboveground biomass, BGB_u: understory belowground biomass, $PPFD_{bc}$: below-canopy instantaneous daytime photosynthetic photon flux density, VPD_{bc}: below-canopy vapor pressure deficit, Ta_{bc}: below-canopy air temperature, Ts_{10}: soil temperature at 10 cm depth and SWC_5: soil volumetric water content at 5 cm depth. Dots and lines represent the 2-year (2017–2018) mean annual (i.e., stand age, AGB_t, AGB_u, and BGB_u) and growing season (i.e., LAI_{max}, $PPFD_{bc}$, VPD_{bc}, Ta_{bc}, Ts_{10}, and SWC_5) values and linear regression fit line, respectively. The gray area refers to the 95 % confidence interval for the regression line. Coefficient of determination (R^2) and p-value are shown. $n = 50$ forest stands.
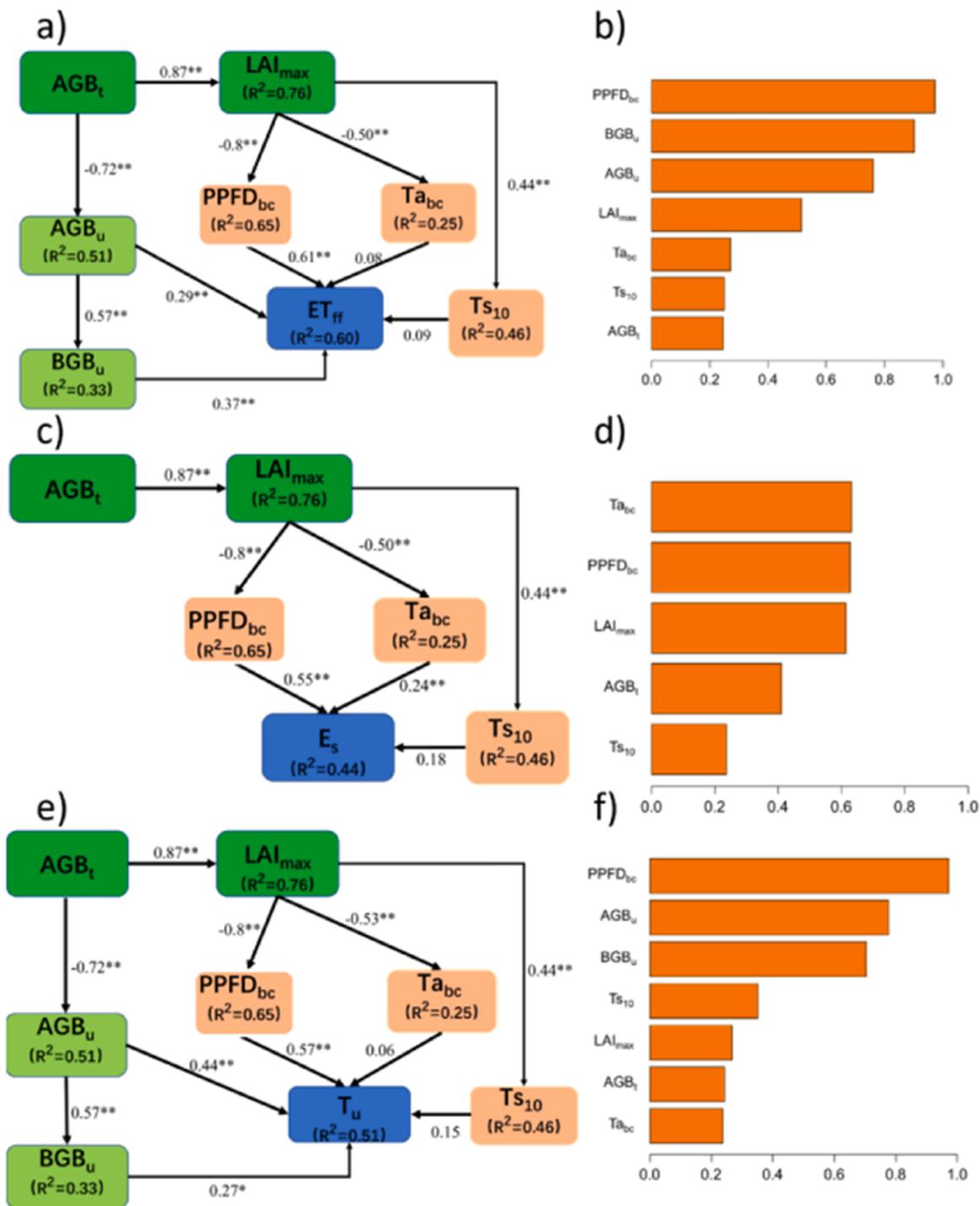
Fig. 7. Structural equation model revealing the impacts of tree aboveground biomass (AGB$_t$), understory aboveground biomass (AGB$_u$), understory belowground biomass (BGB$_u$), leaf area index at peak growing season (LAI$_{max}$), below-canopy instantaneous photosynthetic photon flux density (PPFD$_{bc}$), below-canopy air temperature (Ta$_{bc}$), and soil temperature at 10 cm depth (Ts$_{10}$) on spatial variations of a) forest-floor evapotranspiration (ET$_{ff}$), c) soil evaporation (E$_s$), and e) forest-floor understory transpiration (T$_u$) across the 50 forest stands. Significance level was set at $\alpha = 0.05$. Data based on 2-year (2017– 2018) mean annual (i.e., AGB$_t$, AGB$_u$, and BGB$_u$) and growing season (i.e., LAI$_{max}$, PPFD$_{bc}$, Ta$_{bc}$, and Ts$_{10}$) values. Numbers beside the arrows are standardized coefficients. R^2 refers to the variation degree of the variable interpreted by all paths from the combination from the fixed and random effects. *p-value $\leq$ 0.05, **p-value $\leq$ 0.01. Model-averaged importance of the predictors on b) forest-floor evapotranspiration (ET$_{ff}$), d) soil evaporation (E$_s$), and f) forest-floor understory transpiration (T$_u$).

climate and/or stand structure), measurement methods, and spatial scales, highlighting the need to better understand the underlying mechanisms that cause divergence in ET$_{ff}$ across boreal forest stands.

Studies conducted in boreal forest stands partitioning whole-ecosystem ET into its component fluxes have shown that the contributions of transpiration and evaporation to ET ranged from 47 % to 83 %

and 17 % to 53 %, respectively (Miralles et al., 2011; Schlesinger and Jasechko, 2014; Zhou et al., 2016). This demonstrates the large variability in the contribution of T to the forest water cycle in these high latitude ecosystems. Accordingly, T$_u$/ET$_{ff}$ and E$_s$/ET$_{ff}$ varied greatly across the 50 forest stands, ranging from 19 % to 83 % and from 38 % to 85 %, respectively. To our surprise, we did not identify any dominant

environmental and/or stand structural variable that controlled the T_u/ET_{ff} and E_s/ET_{ff} ratios (Fig. S7), suggesting that various factors may have partly counterbalancing effects on T_u and E_s. This further highlights the complexity of regulating mechanisms, which poses a challenge in predicting spatio-temporal variations in the separate contributions of T_u and E_s across the boreal forest landscape.

4.2. Environmental controls on temporal variation of ET_{ff}, E_s, and T_u

Numerous studies have shown that the main environmental factors affecting tree transpiration on a temporal scale are air temperature (which regulates the atmospheric vapor pressure deficit), energy supply from solar radiation, and soil water availability (Monteith,1973, 1965; Balandier et al., 2022; Gao et al., 2022; Sabater et al., 2020). However, only a few studies have explored how these factors regulate ET_{ff}, E_s, and T_u at the forest-floor interface. The asymptotic relationship between forest-floor H_2O fluxes with below-canopy photosynthetic photon flux density and below-canopy vapor pressure deficit observed in our study may be attributed to the fact that high radiation and vapor pressure deficit values coincided with warm and dry summer conditions. During such periods, constraints from reduced soil water content may limit the response of E_s to radiation (Heijmans et al., 2004; Magliano et al., 2017). In contrast, the saturation response of T_u to radiation and vapor pressure deficit may be mediated by the down-regulation of stomatal conductance at high radiation, which coincides with high temperature and vapor pressure deficit (Chen et al., 2024). Therefore, it is critical to understanding this dual response of the two ET_{ff} component fluxes to radiative energy supply to predict the variation in the bulk response of ET_{ff} across diverse boreal forest stands.

Our study encompassed a historic drought event in the 2018 growing season, during which we observed a considerable increase in ET_{ff} despite a decrease in soil water content. This observation may seem counter-intuitive, but it could be explained by the opposite seasonal below-canopy variation of photosynthetic photon flux density, air temperature, and soil temperature compared to soil water content. These variables showed a maximum and minimum during the peak summer, respectively (Fig. S4), resulting also in a negative relationship between ET_{ff} and soil water content (Table 2). Even during this exceptionally dry summer, the seasonal variations in ET_{ff} and its components were primarily regulated by radiation and temperature, without being constrained by vapor pressure deficit or soil water limitation. However, the relatively higher T_u/ET_{ff} compared to E_s/ET_{ff} observed during the 2018 growing season (57 % versus 44 %, respectively) suggests that reduced soil water content may have limited E_s more than T_u during the drought. One possible explanation for the lack of an apparent T_u drought response could be that there was sufficient soil moisture in deeper soil layers to maintain T_u (Chen et al., 2023b). Alternatively, our measurement interval may have been too coarse to capture the peak drought effect on T_u. However, three years of continuous measurements from a network of tree sap flow sensors in a mature stand within the same study catchment showed that drought also did not significantly reduce tree transpiration during the historic drought of 2018 (Gutierrez Lopez et al. 2021). We speculate that soil water in deeper layers, which was likely replenished by several intense thunderstorms during the summer of 2018, remained at a level that did not limit tree and forest-floor understory transpiration rates in this boreal forest landscape.

4.3. Stand structural and environmental controls on spatial variation of ET_{ff}, E_s, and T_u

Our results suggest that stand structural properties, including stand age, leaf area index, and above- and belowground understory biomasses, significantly affected the spatial variability of forest-floor H_2O fluxes across the managed forest landscape (Figs. 6 and 7). The effect of tree canopy development, which involves an increase in tree aboveground biomass and leaf area index is primarily mediated by regulating the

below-canopy photosynthetic photon flux density through canopy shading. This, in turn, modulates the forest-floor understory development by altering the competition for resources (Martínez-García et al., 2022), and consequently modifying the control of above- and below-ground biomasses on T_u (Baldocchi et al., 1997; Constantin et al., 1999; Heijmans et al., 2004). Similarly, tree canopy development primarily regulated E_s by modulating below-canopy photosynthetic photon flux density through canopy shading (Benyon and Doody, 2015; Kassuelke et al., 2022). Together, this may lead to complex interactions between overstory and understory controls on ET_{ff}, with their relative importance likely shifting during stand development (Widenfalk and Weslien, 2009; Petersson et al., 2019).

In comparison to spruce trees, pine trees have less dense canopy structure. This has an impact on the amount of light and water that reaches the forest-floor (Martínez-García et al 2022). In addition, spruce stands may experience thicker organic soil layers due to higher tree canopy biomass and litter production, which can affect soil moisture dynamics (Barbier et al., 2008). Furthermore, it is common for spruce trees to have shallower roots than the pine trees, making them less able to access water in deeper soils. This fact can result in reduced transpiration during dry periods (Iida et al., 2009; Matyssek et al., 2009; Gebauer et al., 2015). Given these various tree species-specific characteristics, it was surprising that we did not observe any significant effect of tree species on ET_{ff}, E_s, or T_u in our study. It is possible that the dominant effect of stand structure counterbalances effects of other secondary controlling factors, which could explain the lack of a tree species effect on ET_{ff}, E_s, and T_u across the forest landscape.

Soil type may also affect ET_{ff} (Ohta et al., 2001; Kassuelke et al., 2022). Specifically, till soils, which are located in upslope terrain positions, have lower mineral soil depth, pH levels, clay content, and water retention compared to the sediment soils found in valley fills and fluvial systems (Marek and Richardson, 2020; Larson et al., 2022, 2023). Soils with high water-holding capacity may support higher E_s, but also allow the forest-floor understory to access sufficient water even under arid or water-deficient conditions, thereby maintaining higher T_u (Macfarlane et al., 2010). Our observation of higher E_s from sediment soils indicates an effect of soil type. However, since sediment soils mostly occurred in pine stands with less dense canopies, resulting in warmer soil temperatures and higher below-canopy radiation levels, this may have also contributed to higher E_s. Therefore, the observed effect may be attributed, at least partially, to differences in canopy structure rather than soil type. Overall, our results suggest that relative to stand structural properties, soil factors played a relatively minor role in regulating ET_{ff} and its component fluxes across the studied forest landscape.

Currently, there is a trend in Europe to align forest management for reaching various goals, including sustainable development, ecological values, and economic efficiency (Heinonen et al., 2017; Jacobsen et al., 2018). This includes improving harvesting efficiency and extending forest rotations (Gustafsson et al., 2010; Lämås et al., 2015; Kauppi et al., 2022). In terms of forest-floor understory vegetation, the focus is commonly placed on increasing biodiversity and improving ecosystem resilience to better adapt to climate change and other environmental stressors (Deng et al., 2023). This also has implications for the composition and structure of the forest-floor understory vegetation, which can significantly affect the magnitude of ET_{ff} and its component fluxes. In Fennoscandia, there is currently a strong interest in transitioning from rotation-forestry to continuous cover forestry (Peura et al., 2018). The latter management strategy typically retains a greater standing tree biomass. This can modify below-canopy radiation and temperature through increased shading, as well as forest-floor understory vegetation via enhanced competition (Kuuluvainen et al., 2012; Calladine et al., 2015). Based on our results, we note that increasing the share of continuous tree cover may have significant implications for ET_{ff}, i.e., likely resulting in a reduction of both T_u and E_s. Hence, changes in forest management may have important consequences for the boreal forest water cycle.

5. Conclusions

The spatio-temporal variability of ET_{ff} and its component fluxes, E_s and T_u, was analyzed in 50 forest stands across a managed boreal forest landscape. Our results indicate that ET_{ff}, E_s, and T_u exhibited a manifold variability at the managed landscape-level, with distinct controlling factors at both spatial and temporal scales. Specifically, below-canopy temperature regulated the seasonal variations, while below-canopy radiation and forest-floor understory biomass were the primary factors determining the spatial variability at the landscape-scale. Our study thus highlights that the dynamics of ET_{ff} in the managed boreal forest landscape are jointly controlled by environmental and stand structural factors. This finding has significant implications for the dynamics of ET_{ff} and the partitioning of forest water balance in boreal forests in response to forest management and climate change.

CRediT authorship contribution statement

Zifan Guo: Conceptualization, Formal analysis, Investigation, Writing – original draft, Visualization. **Hengshuo Zhang:** Conceptualization, Formal analysis, Investigation, Writing – review & editing. **Eduardo Martínez-García:** Methodology, Data curation, Investigation, Writing – review & editing. **Xizhi Lv:** Supervision, Writing – review & editing. **Hjalmar Laudon:** Resources, Writing – review & editing. **Mats B. Nilsson:** Methodology, Writing – review & editing. **Matthias Peichl:** Conceptualization, Methodology, Data curation, Investigation, Resources, Writing – review & editing, Supervision, Project administration, Funding acquisition.

Declaration of competing interest

The authors declare that they have no known competing financial interests or personal relationships that could have appeared to influence the work reported in this paper.

Acknowledgements

Supplementary materials

Supplementary material associated with this article can be found, in the online version, at doi:10.1016/j.agrformet.2024.110316.

Data availability

The data that support the findings of this study are available from the authors upon reasonable request.

References

Balandier, P., Gobin, R., Prévosto, B., Korboulewsky, N., 2022. The contribution of understorey vegetation to ecosystem evapotranspiration in boreal and temperate forests: a literature review and analysis. Eur. J. For. Res. 141 (6), 979–997.

Baldocchi, D.D., Vogel, C.A., 1996. Energy and CO_2 flux densities above and below a temperate broad-leaved forest and a boreal pine forest. Tree Physiol. 16 (1-2), 5–16.

Baldocchi, D.D., Vogel, C.A., Hall, B., 1997. Seasonal variation of energy and water vapor exchange rates above and below a boreal jack pine forest canopy. J. Geophys. Res.: Atmos. 102 (D24), 28939–28951.

Barbier, S., Gosselin, F., Balandier, P., 2008. Influence of tree species on understory vegetation diversity and mechanisms involved—A critical review for temperate and boreal forests. Forest Ecol. Manag. 254 (1), 1–15.

Barker, C.A., Amiro, B.D., Kwon, H., Ewers, B.E., Angstmann, J.L., 2009. Evapotranspiration in intermediate-aged and mature fens and upland black spruce boreal forests. Ecohydrology 2 (4), 462–471.

Benyon, R.G., Doody, T.M., 2015. Comparison of interception, forest floor evaporation and transpiration in *Pinus radiata* and *Eucalyptus globulus* plantations. Hydrol. Processes 29 (6), 1173–1187.

Bosch, D.D., Marshall, L.K., Teskey, R., 2014. Forest transpiration from sap flux density measurements in a Southeastern Coastal Plain riparian buffer system. Agric. For. Meteorol. 187, 72–82.

Calladine, J., Bray, J., Broome, A., Fuller, R.J., 2015. Comparison of breeding bird assemblages in conifer plantations managed by continuous cover forestry and clearfelling. Forest Ecol. Manag. 344, 20–29.

Chen, L., Zhang, Z., Li, Z., Tang, J., Caldwell, P., Zhang, W., 2011. Biophysical control of whole tree transpiration under an urban environment in Northern China. J. Hydrol. 402 (3), 388–400.

Chen, S., Chen, Z., Kong, Z., Zhang, Z., 2023a. The increase of leaf water potential and whole-tree hydraulic conductance promotes canopy conductance and transpiration of Pinus tabulaeformis during soil droughts. Trees 37 (1), 41–52.

Chen, S., Wei, W., Tong, B., Chen, L., 2023b. Effects of soil moisture and vapor pressure deficit on canopy transpiration for two coniferous forests in the Loess Plateau of China. Agric. For. Meteorol. 339, 109581.

Chen, S., Zhang, Z., Chen, Z., Xu, H., Li, J., 2024. Responses of canopy transpiration and conductance to different drought levels in Mongolian pine plantations in a semiarid urban environment of China. Agric. For. Meteorol. 347, 109897.

Chi, J., Zhao, P., Klosterhalfen, A., Jocher, G., Kljun, N., Nilsson, M.B., Peichl, M., 2021. Forest floor fluxes drive differences in the carbon balance of contrasting boreal forest stands. Agric. For. Meteorol. 306, 108454.

Constantin, J., Grelle, A., Ibrom, A., Morgenstern, K., 1999. Flux partitioning between understorey and overstorey in a boreal spruce/pine forest determined by the eddy covariance method. Agric. For. Meteorol. 98-99, 629–643.

Deng, J., Fang, S., Fang, X., Jin, Y., Kuang, Y., Lin, F., Liu, J., Ma, J., Nie, Y., Ouyang, S., Ren, J., Tie, L., Tang, S., Tan, X., Wang, X., Fan, Z., Wang, Q.-W., Wang, H., Liu, C., 2023. Forest understory vegetation study: current status and future trends. Forestry Research 3, 6.

Gao, G., Wang, D., Zha, T., Wang, L., Fu, B., 2022. A global synthesis of transpiration rate and evapotranspiration partitioning in the shrub ecosystems. J. Hydrol. 606, 127417.

Gebauer, R., Cermák, J., Plichta, R., Spinlerová, Z., Urban, J., Volarík, D., Ceulemans, R., 2015. Within-canopy variation in needle morphology and anatomy of vascular tissues in a sparse Scots pine forest. Trees. 29 (5), 1447–1457.

Gustafsson, L., Kouki, J., Sverdrup-Thygeson, A., 2010. Tree retention as a conservation measure in clear-cut forests of northern Europe: a review of ecological consequences. Scand. J. For. Res. 25 (4), 295–308.

Gutierrez Lopez, J., Tor-Ngern, P., Oren, R., Kozii, N., Laudon, H., Hasselquist, N.J., 2021. How tree species, tree size, and topographical location influenced tree transpiration in northern boreal forests during the historic 2018 drought. Global Change Biol. 27 (13), 3066–3078.

Hamada, S., Ohta, T., Hiyama, T., Kuwada, T., Takahashi, A., Maximov, T.C., 2004. Hydrometeorological behaviour of pine and larch forests in eastern Siberia. Hydrol. Processes 18 (1), 23–39.

Hamel, P., McHugh, I., Coutts, A., Daly, E., Beringer, J., Fletcher Tim, D., 2015. Automated chamber system to measure field evapotranspiration rates. J. Hydrol. Eng. 20 (2), 04014037.

Hao, S., Jia, X., Mu, Y., Zha, T., Qin, S., Liu, P., Tian, Y., Qi, J., Zhao, H., Li, X., 2023. Canopy greenness, atmospheric aridity, and large rain events jointly regulate evapotranspiration partitioning in a temperate semiarid shrubland. Agric. For. Meteorol. 333, 109425.

Heijmans, M.M.P.D., Arp, W.J., Chapin, F.S., 2004. Carbon dioxide and water vapour exchange from understory species in boreal forest. Agric. For. Meteorol. 123 (3-4), 135–147.

Heinonen, T., Pukkala, T., Mehtätalo, L., Asikainen, A., Kangas, J., Peltola, H., 2017. Scenario analyses for the effects of harvesting intensity on development of forest resources, timber supply, carbon balance and biodiversity of Finnish forestry. Forest Policy and Economics 80, 80–98.

Helbig, M., Waddington, J.M., Alekseychik, P., Amiro, B.D., Aurela, M., Barr, A.G., Black, T.A., Blanken, P.D., Carey, S.K., Chen, J., Chi, J., Desai, A.R., Dunn, A., Euskirchen, E.S., Flanagan, L.B., Forbrich, I., Friborg, T., Grelle, A., Harder, S., Heliasz, M., Humphreys, E.R., Ikawa, H., Isabelle, P.-E., Iwata, H., Jassal, R., Korkiakoski, M., Kurbatova, J., Kutzbach, L., Lindroth, A., Löfvenius, M.O., Lohila, A., Mammarella, I., Marsh, P., Maximov, T., Melton, J.R., Moore, P.A., Nadeau, D.F., Nicholls, E.M., Nilsson, M.B., Ohta, T., Peichl, M., Petrone, R.M., Petrov, R., Prokushkin, A., Quinton, W.L., Reed, D.E., Roulet, N.T., Runkle, B.R.K., Sonnentag, O., Strachan, I.B., Taillardat, P., Tuittila, E.-S., Tuovinen, J.-P., Turner, J., Ueyama, M., Varlagin, A., Wilmking, M., Wofsy, S.C., Zyrianov, V., 2020. Increasing contribution of peatlands to boreal evapotranspiration in a warming climate. Nat. Clim. Change 10 (6), 555–560.

Iida, S.i., Ohta, T., Matsumoto, K., Nakai, T., Kuwada, T., Kononov, A.V., Maximov, T.C., van der Molen, M.K., Dolman, H., Tanaka, H., Yabuki, H., 2009. Evapotranspiration

from understory vegetation in an eastern Siberian boreal larch forest. Agric. For. Meteorol. 149 (6-7), 1129–1139.

Iqbal, S., Zha, T., Jia, X., Hayat, M., Qian, D., Bourque, C.P.A., Tian, Y., Bai, Y., Liu, P., Yang, R., Khan, A., 2021. Interannual variation in sap flow response in three xeric shrub species to periodic drought. Agric. For. Meteorol. 297, 108276.

Jacobsen, J.B., Jensen, F., Thorsen, B.J., 2018. Forest value and optimal rotations in continuous cover forestry. Environ Resource Econ 69 (4), 713–732.

Jin, C., Zha, T., Bourque, C.P.A., Liu, P., Jia, X., Zhang, F., Yu, H., Tian, Y., Li, X., Kang, X., Guo, X., Wang, N., 2023. Multi-year trends and interannual variation in ecosystem resource use efficiencies in a young mixedwood plantation in northern China. Agric. For. Meteorol. 330, 109318.

Kassuelke, S.R., Dymond, S.F., Feng, X., Savage, J.A., Wagenbrenner, J.W., 2022. Understory evapotranspiration rates in a coast redwood forest. Ecohydrology 15 (3), e2404.

Kauppi, P.E., Stål, G., Arnesson-Ceder, L., Hallberg Sramek, I., Hoen, H.F., Svensson, A., Wernick, I.K., Högberg, P., Lundmark, T., Nordin, A., 2022. Managing existing forests can mitigate climate change. Forest Ecol. Manag. 513, 120186.

Kelliher, F.M., Hollinger, D.Y., Schulze, E.D., Vygodskaya, N.N., Byers, J.N., Hunt, J.E., McSeveny, T.M., Milukova, I., Sogatchev, A., Varlargin, A., Ziegler, W., Arneth, A., Bauer, G., 1997. Evaporation from an eastern Siberian larch forest. Agric. For. Meteorol. 85 (3), 135–147.

Kelliher, F.M., Lloyd, J., Arneth, A., Byers, J.N., McSeveny, T.M., Milukova, I., Grigoriev, S., Panfyorov, M., Sogatchev, A., Varlargin, A., Ziegler, W., Bauer, G., Schulze, E.D., 1998. Evaporation from a central Siberian pine forest. J. Hydrol. 205 (3), 279–296.

Kelliher, F.M., Whitehead, D., McAneney, K.J., Judd, M.J., 1990. Partitioning evapotranspiration into tree and understorey components in two young pinus radiata D. Don stands. Agric. For. Meteorol. 50 (3), 211–227.

Kotani, A., Kononov, A.V., Ohta, T., Maximov, T.C., 2014. Temporal variations in the linkage between the net ecosystem exchange of water vapour and CO_2 over boreal forests in eastern Siberia. Ecohydrology 7 (2), 209–225.

Kozii, N., Haahti, K., Tor-ngern, P., Chi, J., Hasselquist, E.M., Laudon, H., Launiainen, S., Oren, R., Peichl, M., Wallerman, J., Hasselquist, N.J., 2020. Partitioning growing season water balance within a forested boreal catchment using sap flux, eddy covariance, and a process-based model. Hydrol. Earth Syst. Sci. 24 (6), 2999–3014.

Kuuluvainen, T., Tahvonen, O., Aakala, T., 2012. Even-aged and uneven-aged forest management in boreal Fennoscandia: a review. Ambio 41 (7), 720–737.

Lafleur, P.M., Rouse, W.R., 1988. The influence of surface cover and climate on energy partitioning and evaporation in a subarctic wetland. Boundary Layer Meteorol. 44 (4), 327–347.

Lämås, T., Sandström, E., Jonzén, J., Olsson, H., Gustafsson, L., 2015. Tree retention practices in boreal forests: what kind of future landscapes are we creating? Scand. J. For. Res. 30 (6), 526–537.

Larson, J., Lidberg, W., Ågren, A.M., Laudon, H., 2022. Predicting soil moisture conditions across a heterogeneous boreal catchment using terrain indices. Hydrol. Earth Syst. Sci. 26 (19), 4837–4851.

Larson, J., Wallerman, J., Peichl, M., Laudon, H., 2023. Soil moisture controls the partitioning of carbon stocks across a managed boreal forest landscape. Sci. Rep. 13 (1), 14909.

Laudon, H., Hasselquist, E.M., Peichl, M., Lindgren, K., Sponseller, R., Lidman, F., Kuglerová, L., Hasselquist, N.J., Bishop, K., Nilsson, M.B., Ågren, A.M., 2021. Northern landscapes in transition: Evidence, approach and ways forward using the Krycklan Catchment Study. Hydrol. Processes 35, e14170.

Liu, J., Cheng, F., Munger, W., Jiang, P., Whitby, T.G., Chen, S., Ji, W., Man, X., 2020a. Precipitation extremes influence patterns and partitioning of evapotranspiration and transpiration in a deciduous boreal larch forest. Agric. For. Meteorol. 287, 107936.

Liu, P., Black, T.A., Jassal, R.S., Zha, T., Nesic, Z., Barr, A.G., Helgason, W.D., Jia, X., Tian, Y., Stephens, J.J., Ma, J., 2019. Divergent long-term trends and interannual variation in ecosystem resource use efficiencies of a southern boreal old black spruce forest 1999-2017. Global Change Biol. 25 (9), 3056–3069.

Liu, Y., Kumar, M., Katul, G.G., Feng, X., Konings, A.G., 2020b. Plant hydraulics accentuates the effect of atmospheric moisture stress on transpiration. Nat. Clim. Change 10 (7), 691–695.

Liu, Z., Wang, Y., Yu, P., Xu, L., Yu, S., 2022. Environmental and canopy conditions regulate the forest floor evapotranspiration of larch plantations. For. Ecosyst. 9, 100058.

Livingston, G.P., Hutchinson, G.L., 1995. Enclosure-based measurement of trace gas exchange: Applications and sources of error. In: P.A. Matson, R.C. Harriss (Editors), Biogenic trace gases: Measuring emissions from soil and water. Blackwell Science Ltd., Oxford, UK, pp. 15–51.

Lyu, J.L., He, Q.Y., Chen, Q.W., Cheng, R.R., Li, G.Q., Otsuki, K., Yamanaka, N., Du, S., 2022. Distinct transpiration characteristics of black locust plantations acclimated to semiarid and subhumid sites in the Loess Plateau, China. Agric. Water Manag 262, 107402.

Macfarlane, C., Bond, C., White, D.A., Grigg, A.H., Ogden, G.N., Silberstein, R., 2010. Transpiration and hydraulic traits of old and regrowth eucalypt forest in southwestern Australia. Forest Ecol. Manag. 260 (1), 96–105.

Magliano, P.N., Giménez, R., Houspanossian, J., Páez, R.A., Nosetto, M.D., Fernández, R.J., Jobbágy, E.G., 2017. Litter is more effective than forest canopy reducing soil evaporation in Dry Chaco rangelands. Ecohydrology e1879.

Marek, R.S., Richardson, J.B., 2020. Investigating surficial geologic controls on soil properties, inorganic nutrient uptake, and northern hardwood growth in western massachusetts, USA. J. Soil Sci. Plant Nutr. 20 (3), 901–911.

Marques, T.V., Mendes, K., Mutti, P., Medeiros, S., Silva, L., Perez-Marin, A.M., Campos, S., Lúcio, P.S., Lima, K., dos Reis, J., Ramos, T.M., da Silva, D.F., Oliveira, C.P., Costa, G.B., Antonino, A.C.D., Menezes, R.S.C., Santos e Silva, C.M.,

Bezerra, B., 2020. Environmental and biophysical controls of evapotranspiration from Seasonally Dry Tropical Forests (Caatinga) in the Brazilian Semiarid. Agric. For. Meteorol. 287, 107957.

Martínez-García, E., Nilsson, M.B., Laudon, H., Lundmark, T., Fransson, J.E.S., Wallerman, J., Peichl, M., 2022. Overstory dynamics regulate the spatial variability in forest-floor CO_2 fluxes across a managed boreal forest landscape. Agric. For. Meteorol. 318, 108916.

Matyssek, R., Wieser, G., Patzner, K., Blaschke, H., Häberle, K.H., 2009. Transpiration of forest trees and stands at different altitude: consistencies rather than contrasts? Eur. J. For. Res. 128 (6), 579–596.

McLaren, J.D., Arain, M.A., Khomik, M., Peichl, M., Brodeur, J.J., 2008. Water flux components and soil water-atmospheric controls in a temperate pine forest growing in a well drained sandy soil. J. of Geophys. Res. Biogeosci. 113. G04031.

McLeod, M.K., Daniel, H., Faulkner, R., Murison, R., 2004. Evaluation of an enclosed portable chamber to measure crop and pasture actual evapotranspiration at small scale. Agric. Water Manage. 67 (1), 15–34.

Miralles, D.G., De Jeu, R.A.M., Gash, J.H., Holmes, T.R.H., Dolman, A.J., 2011. Magnitude and variability of land evaporation and its components at the global scale. Hydrol. Earth Syst. Sci. 15 (3), 967–981.

Monteith, J.L., 1973. Principles of Environmental Physics.

Monteith, J.L., Unsworth, M.H., 1990. Principles of Environmental Physics, 2nd ed.

Monteith, J.L., 1965. Evaporation and Environment. 19th Symposia of the Society for Experimental Biology, 19. University Press, Cambridge, pp. 205–234.

Niu, X.D., Liu, S.R., 2022. Environmental and stomatal control on evapotranspiration in a natural oak forest. Ecohydrology 15, e2423.

Numata, I., Khand, K., Kjaersgaard, J., Cochrane, M.A., Silva, S.S., 2021. Forest evapotranspiration dynamics over a fragmented forest landscape under drought in southwestern Amazonia. Agric. For. Meteorol. 306, 108446.

Ohta, T., Hiyama, T., Tanaka, H., Kuwada, T., Maximov, T.C., Ohata, T., Fukushima, Y., 2001. Seasonal variation in the energy and water exchanges above and below a larch forest in eastern Siberia. Hydrol. Processes 15 (8), 1459–1476.

Pan, Y., Birdsey, R.A., Fang, J., Houghton, R., Kauppi, P.E., Kurz, W.A., Phillips, O.L., Shvidenko, A., Lewis, S.L., Canadell, J.G., Ciais, P., Jackson, R.B., Pacala, S.W., McGuire, A.D., Piao, S., Rautiainen, A., Sitch, S., Hayes, D., 2011. A large and persistent carbon sink in the world's forests. Science 333 (6045), 988–993.

Williams, A.P., Allen, C.D., Macalady, A.K., Griffin, D., Woodhouse, C.A., Meko, D.M., Swetnam, T.W., Rauscher, S.A., Seager, R., Grissino-Mayer, H.D., Dean, J.S., Cook, E.R., Gangodagamage, C., Cai, M., McDowell, N.G., 2013. Temperature as a potent driver of regional forest drought stress and tree mortality. Nat. Clim. Change 3 (3), 292–297.

Peichl, M., Martinez-Garcia, E., Fransson, J.E.S., Wallerman, J., Laudon, H., Lundmark, T., Nilsson, M.B., 2023a. Landscape-variability of the carbon balance across managed boreal forests. Global Change Biol. 29 (4), 1119–1132.

Peichl, M., Martinez-Garcia, E., Fransson, J.E.S., Wallerman, J., Laudon, H., Lundmark, T., Nilsson, M.B., 2023b. On the uncertainty in estimates of the carbon balance recovery time after forest clear-cutting. Global Change Biol. 00, 1–3.

Penman, H.L., 1963. Vegetation and hydrology. Tech. Comm. No. 53. Commonwealth Bureau of Soils 125.

Penman, H.L., Keen, B.A., 1948. Natural evaporation from open water, bare soil and grass. Proceedings of the Royal Society of London. Series A. Mathematical and Physical Sciences 193 (1032), 120–145.

Petersson, L., Holmström, E., Lindbladh, M., Felton, A., 2019. Tree species impact on understory vegetation: Vascular plant communities of Scots pine and Norway spruce managed stands in northern. Europe. Forest Ecol. Manag. 448, 330–345.

Peura, M., Burgas, D., Eyvindson, K., Repo, A., Mönkkönen, M., 2018. Continuous cover forestry is a cost-efficient tool to increase multifunctionality of boreal production forests in Fennoscandia. Biol. Conserv. 217, 104–112.

Sabater, A.M., Ward, H.C., Hill, T.C., Gornall, J.L., Wade, T.J., Evans, J.G., Prieto-Blanco, A., Disney, M., Phoenix, G.K., Williams, M., Huntley, B., Baxter, R., Mencuccini, M., Poyatos, R., 2020. Transpiration from subarctic deciduous woodlands: Environmental controls and contribution to ecosystem evapotranspiration. Ecohydrology 13 (3), e2190.

Schlesinger, W.H., Jasechko, S., 2014. Transpiration in the global water cycle. Agric. For. Meteorol. 189-190, 115–117.

Seemann, J., Chirkov, Y.I., Lomas, J., Primault, B., 1979. Agrometeorology. Springer Verlag, Berlin, Heidelberg.

Shuttleworth, W.J. 1993. Evaporation. In: D. R. Maidment (ed) Handbook of Hydrology. McGraw Hill, New York: 4.1-4.53.

Wang, T.X., Zhang, H.Y., Zhao, J.J., Guo, X.Y., Xiong, T., Wu, R.H., 2021. Shifting contribution of climatic constraints on evapotranspiration in the boreal forest. Earths-Future 9 (8) e2021EF002104.

Widenfalk, O., Weslien, J., 2009. Plant species richness in managed boreal forests—Effects of stand succession and thinning. Forest Ecol. Manag. 257 (5), 1386–1394.

Yang, Y., Anderson, M., Gao, F., Hain, C., Noormets, A., Sun, G., Wynne, R., Thomas, V., Sun, L., 2020. Investigating impacts of drought and disturbance on evapotranspiration over a forested landscape in North Carolina, USA using high spatiotemporal resolution remotely sensed data. Remote Sens. Environ. 238, 111018.

Zha, T.S., Barr, A.G., Bernier, P.Y., Lavigne, M.B., Trofymow, J.A., Amiro, B.D., Arain, M.A., Bhatti, J.S., Black, T.A., Margolis, H.A., McCaughey, J.H., Xing, Z.S., Van Rees, K.

C.J., Coursolle, C., 2013. Gross and aboveground net primary production at Canadian forest carbon flux sites. Agric. For. Meteorol. 174-175, 54–64.

Zhang, Y.Q., Chiew, F.H.S., Peña-Arancibia, J., Sun, F.B., Li, H.X., Leuning, R., 2017. Global variation of transpiration and soil evaporation and the role of their major climate drivers. J. Geophys. Res.-Atmospheres 122 (13), 6868–6881.

Zhou, S., Yu, B., Zhang, Y., Huang, Y., Wang, G., 2016. Partitioning evapotranspiration based on the concept of underlying water use efficiency. Water Resour. Res. 52 (2), 1160–1175.